Olefin Production by Cofeeding Methanol and *n*-Butane: Kinetic Modeling Considering the Deactivation of HZSM-5 Zeolite

Diana Mier, Ana G. Gayubo, Andres T. Aguayo, Martin Olazar, and Javier Bilbao
Departamento de Ingeniería Química, Universidad del País Vasco, Apartado 644, 48080 Bilbao, Spain

DOI 10.1002/aic.12471
Published online November 29, 2010 in Wiley Online Library (wileyonlinelibrary.com).

The joint transformation of methanol and n*-butane fed into a fixed-bed reactor on a HZSM-5 zeolite catalyst has been studied under energy neutral conditions (methanol/* n*-butane molar ratio of 3/1). The kinetic scheme of lumps proposed integrates the reaction steps corresponding to the individual reactions (cracking of* n*-butane and MTO process at high-temperature) and takes into account the synergies between the steps of both reactions. The deactivation by coke deposition has been quantified by an expression dependent on the concentration of the components in the reaction medium, which is evidence that oxygenates are the main coke precursors. The concentration of the components in the reaction medium (methanol, dimethyl ether,* n*-butane, C_2—C_4 paraffins, C_2—C_4 olefins, C_5—C_{10} lump, and methane) is satisfactorily calculated in a wide range of conditions (between 400 and 550°C, up to 9.5 (g of catalyst) h (mol $CH_2)^{-1}$ and with a time on stream of 5 h) by combining the equation of deactivation with the kinetic model of the main integrated process.* © 2010 American Institute of Chemical Engineers *AIChE J*, 57: 2841–2853, 2011

Keywords: kinetic model, HZSM-5 zeolite, methanol, n*-butane cracking, MTO process, catalyst deactivation*

Introduction

The joint transformation of paraffins and methanol on a HZSM-5 zeolite catalyst has been called coupled methanol-hydrocarbon cracking (CMHC) process in the literature, being an interesting route for obtaining C_2—C_4 olefins from both secondary interest streams in refineries (light paraffins) and methanol.[1–3] Methanol can be obtained by gasification of sources other than oil: natural gas, coal, and lignocellulosic biomass; the latter contributing to the net reduction of CO_2 emissions.[4] The CMHC process is complementary to the steam cracking of naphtha and the methanol to olefins (MTO) process, which together with fluid catalytic cracking (FCC) produces most of the olefins.[5,6]

Correspondence concerning this article should be addressed to D. Mier at diana.mier@ehu.es.

The integration of paraffin cracking (endothermic) and methanol transformation (exothermic) in the same reactor allows working without supplying or removing heat, which is a determining factor in the two individual reactions. Catalysts prepared based on HZSM-5 zeolites have turned out to be active for paraffin cracking.[7–9] Moreover, although the behavior of HZSM-5 zeolite in the transformation of methanol into olefins (MTO process)[10–12] is well-known, it is performed on SAPO-34 catalysts due to their higher-selectivity to olefins. Nevertheless, the deactivation of the latter by coke is more rapid, given that H-SAPO34 has a 3-D cage structure with 3.8 × 3.8 Å framework dimensions, whereas HZSM-5 has a 3-D 10-ring structure with 5.1 × 5.5 and 5.3 × 5.6 Å framework dimensions.[13,14]

The cracking of both paraffins and *n*-butane nonetheless requires higher-temperatures (>450°C) than those of the MTO process and sites with higher-acid strength (not

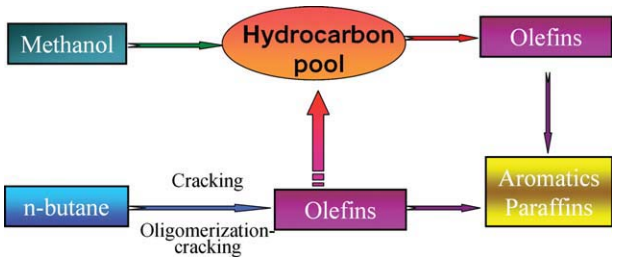

Figure 1. Hydrocarbon pool mechanism activation in methanol transformation by cofeeding *n*-butane.

[Color figure can be viewed in the online issue, which is available at wileyonlinelibrary.com.]

advisable in the MTO process for minimizing the reactions leading to aromatics). Furthermore, the integrated process is carried out with considerable water content in the reaction medium (product of methanol dehydration), which together with high-temperatures is a challenge for the hydrothermal stability of the HZSM-5 zeolite catalyst.[11,15,16] Catalyst hydrothermal stability has been improved by doping the HZSM-5 zeolite with Fe,[17] and agglomerating with bentonite and alumina.[18,19]

The integration of both reactions schematized in Figure 1 is effective for increasing the yield of olefins over those corresponding to the two individual reactions, which is explained by the following findings based on synergies between the kinetic schemes of the two reactions:[20] (i) olefins formed at the initial section of the reactor in *n*-butane cracking activate the autocatalytic steps for methanol transformation, following the well-established "hydrocarbon pool" mechanism originally proposed for SAPO-34 catalyst, which establishes that methylbenzenes are the main reactive species;[12,21–25] (ii) the incorporation of these olefins in the "hydrocarbon pool" maintains the reactivity of methylbenzenes released by the olefins, which delays the formation of polymethylbenzenes that are the precursors of polyaromatic coke;[26,27] (iii) water formation in methanol transformation inhibits the steps for *n*-butane cracking but also deactivation by coke, given that water adsorption on the active sites competes with coke precursor adsorption in the coke growing steps.[28,29]

A further fact to be taken into account is that the heat released "*in situ*" in the dehydration of methanol on the same active sites avoids the presumable energy deficiency in the endothermic cracking step. This hypothesis concerning energy compensation has been established to explain also the higher-conversion obtained in the hydrocracking of aromatics in a single step (on bifunctional Pt/HZSM-5 catalysts) compared with the conversion corresponding to the process in two consecutive steps, in which the dehydration is exothermic and the cracking of the resulting cycloalkanes is endothermic.[30,31] Based on the results of the integrated process formed by *n*-hexane and methanol as reactants, Chang et al.[32] postulated that the intermediates (methoxy ions) in the transformation of methanol activate the mechanism of *n*-hexane bimolecular cracking by complementing the monomolecular cracking mechanism that occurs by *n*-hexane protonation on the Brönsted acid sites of the zeolite.

Energy compensation on the acid sites explains that the yields of methane, CO, and CO_2 are lower in the integrated process than in methanol transformation, given that the reactions for the formation of these by-products are favored by temperature.[20] This result is interesting for a higher-upgrading of carbon atoms in the feed.

The aim of this study is to determine a kinetic model that allows quantifying product distribution by paying special attention to C_2—C_4 olefins and considering catalyst deactivation by coke deposition. The hypotheses for the kinetic modeling are based on the kinetic models previously established for each of the two reactions on the same catalyst.[33,34]

Experimental

Reaction equipment and product analysis

The runs have been carried out under atmospheric pressure in the automated reaction equipment described in a previous article.[20] The reactor is made of 316 stainless steel with an internal diameter of 9 mm and 10 cm of effective length. It is located inside a ceramic covered stainless steel cylindrical chamber, which is heated by an electric resistance and can operate at up to 100 atm and 700°C with a catalyst mass of up to 5 g. The bed consists of a mixture of catalyst and inert solid (carborundum with an average particle diameter of 0.16 mm) to ensure bed isothermality and attain sufficient height under low-space-time conditions. The temperature is controlled by a digital TTM-125 Series controller and measured by a thermocouple (K-type) situated in the catalyst bed. Another thermocouple measures temperature in the internal wall of the reactor. There are two other temperature controllers: one for the furnace chamber and the other for the transfer line between the reactor and the micro-GC. The operating variables are controlled by bespoke software version (process@, PID Eng&Tech, Madrid, Spain).

Reaction product samples (diluted in a He stream of 17 $cm^3\ min^{-1}$) are continuously analyzed in a gas chromatograph (Varian CP-4900). The remaining stream of reaction products passes through a Peltier cell at 0°C. The amount of liquid condensate is controlled by a level sensor and the noncondensable gas flow is vented.

The micro-GC (with Star Toolbar software) is provided with three analytical modules and the following columns: Porapak Q (PPQ) (10 m), where the lighter products are separated (CO_2, methane, ethane, ethylene, propane, propylene, methanol, dimethyl ether, water, butanes, and butenes); a molecular sieve (MS-5) (10 m) where H_2, CO, O_2, and N_2 are separated; and 5CB (CPSIL) (8 m), where C_5—C_{10} fraction is separated. The quantification and identification of the compounds was carried out based on calibration standards of known concentration. The balance of atoms (C, H, O) is closed in all runs above 99.5%.

Catalyst

The catalyst has been selected in a previous article, based on the combination of different criteria (activity at zero time on stream, olefin selectivity, deactivation by coke deposition, and hydrothermal stability).[19] The selected catalyst (HZ-30) has been prepared with a HZSM-5 zeolite, with SiO_2/Al_2O_3

= 30, supplied by Zeolyst International in ammonium form, which has been calcined at 570°C to obtain the acid form.

The zeolite has been agglomerated with a bentonite binder (Exaloid, 30 wt%) and alumina (Prolabo, calcined at 1000°C to become inert) as inert charge (45 wt%). The catalyst particles have been obtained by wet extrusion, using a high-pressure hydraulic piston, through 0.8-mm diameter holes. The extrudates are first dried at room-temperature for 24 h, then they are sieved to a particle diameter between 0.15 and 0.3 mm. The particles are dried in an oven at 110°C for 24 h and then calcined at 575°C for 3 h. This temperature is reached following a ramp of 5°C min^{-1}. The agglomeration of the active phases does not significantly reduce acidity but improves the accessibility of the reactants (providing the catalysts with a matrix with meso- and macro-pores), which is essential for reducing the deactivation by coke deposition,[35,36] and increasing hydrothermal stability in the regeneration step by coke combustion.[18] A catalyst without active phase (HZSM-5 zeolite) has been prepared, and the transformation into products has proven to be negligible.

The catalyst allows performing up to 10 reaction-regeneration cycles, without observing irreversible deactivation either in the reaction stage (in which there is considerable water content in the reaction medium) or in the regeneration stage, which is performed *in situ* by coke combustion with air in the reactor at 550°C.[37]

Table 1 set out the physical properties and the acidity values of the catalysts. The porous structure has been determined by N_2 adsorption–desorption (Micromeritics ASAP 2010) and Hg porosimetry (Micromeritics Autopore 9220). The micropore volume corresponds to the active phase, whereas the volume of meso- and macro-pores corresponds to the matrix of the catalyst (bentonite and alumina).

The analysis by transmission electron microscopy (TEM) (Phillips CM 200) of the catalyst has shown that the zeolite crystal size is below this threshold value and is between 10 and 100 nm. The different internal diffusivities of molecules with different sizes and shapes are known to be predominant factor affecting shape selectivity in the intracrystalline channels of small pore zeolites.[38] It has been proven for HZSM-5 zeolite that the rate-determining step of the overall transport of *n*-butane and propanal is intracrystalline diffusion for zeolite crystal sizes between 3 and 6 μm.[39,40] Consequently, the diffusivity of the reaction components is a consequence of the shape selectivity characteristic to the HZSM-5 structure.

The total acidity and acid strength of the catalysts have been determined by monitoring the adsorption–desorption of NH_3, by combining the techniques of thermo-gravimetric analysis and differential scanning calorimetry using a Setaram TG-DSC calorimeter connected on-line with a Thermostar mass spectrometer from Balzers Instruments.[41,42] The Brönsted/Lewis (B/L) acid site ratio has been determined by analyzing the region of 1400–1700 cm^{-1} in the FTIR spectrum of adsorbed pyridine, which has been obtained using a Specac catalytic chamber connected online with a Nicolet 6700 FTIR spectrometer. The Brönsted/Lewis site ratio value at 150°C has been determined from the ratio between the intensity of pyridine adsorption bands at 1545 and 1450 cm^{-1} and taking into account the molar extinction coefficients of both adsorption bands (ε_B = 1.67 cm μmol^{-1} and ε_L = 2.22 cm μmol^{-1}).

Table 1. Physical Properties and Acidity of the Catalyst

Acid strength [kJ (mol of NH_3)$^{-1}$]	120
Total acidity [(mmol of NH_3) g^{-1}]	0.23
d_p (Å)	102
S_{BET} (m^2 g^{-1})	220
V_m (cm^3 g^{-1})	0.044
V_p ($17 < d_p$(Å)< 3000) (cm^3 g^{-1})	0.69
Pore volume distribution (%)	
$<20/20 < d_p$ (Å) $< 500/ > 500$	2.96/46.5/50.5
Brönsted/Lewis site ratio at 150°C	1.5

The coke deposited on the catalyst has been studied by combustion with air in the TG/DSC arrangement described above. Subsequent to a coke aging step in a He stream at 550°C for 30 min (for results to be reproducible), combustion is carried out with 25% O_2 in He, following a ramp of 3°C min^{-1} up to 550°C, and maintaining this temperature for 2 h.[37] Combustion is complete, given that all the carbon in the coke is volatilized as CO_2. Signals corresponding to the presence of other compounds, such as SO_2 or NO×, are insignificant.

Results

Effect of operating conditions

Experiments have been carried out at atmospheric pressure under the following operating conditions: temperature, in the 400–550°C range; space time, up to 9.5 (g of catalyst) h (mol CH_2)$^{-1}$; methanol/*n*-butane molar ratio in the feed, 3 (0.75 in CH_2 equivalent units) which corresponds to conditions of energy compensation (energy neutral reaction) for complete conversion of reactants, as determined in a previous work;[20] time on stream, 5 h.

The compounds in the reaction medium have been quantified by considering the concentration of methanol (M) and dimethyl ether (D), *n*-butane (reactant and product) (B), methane (C) by-product formed by decomposition of methanol and product lumps, olefins (ethylene, propylene and butenes) (O), paraffins (ethane, propane and isobutane) (P), C_{5+} aliphatics, which include all the olefins and paraffins with more than five carbon atoms and BTX aromatics (benzene, toluene, and xylenes). The formation of CO and CO_2 has not been considered, given that their maximum yield is lower than 0.5% (of C transformed) at the maximum temperature, 550°C, and for the minimum value of space time studied.

Figure 2 shows the effect of temperature on the apparent conversion of the feed ((methanol + dimethyl ether)/*n*-butane), for three values of space time. The conversion increases with space time, and for 2.4 and 4.7 (g of catalyst) h (mol CH_2)$^{-1}$ the conversion increases with temperature. For 0.3 (g of catalyst) h (mol CH_2)$^{-1}$, the conversion increases with temperature until 450°C, for higher-temperatures conversion is practically constant. This conversion been calculated as the fraction of the combined molar flow rate in the feed that has been transformed

$$X = \frac{F_0 - F_e}{F_0} \quad (1)$$

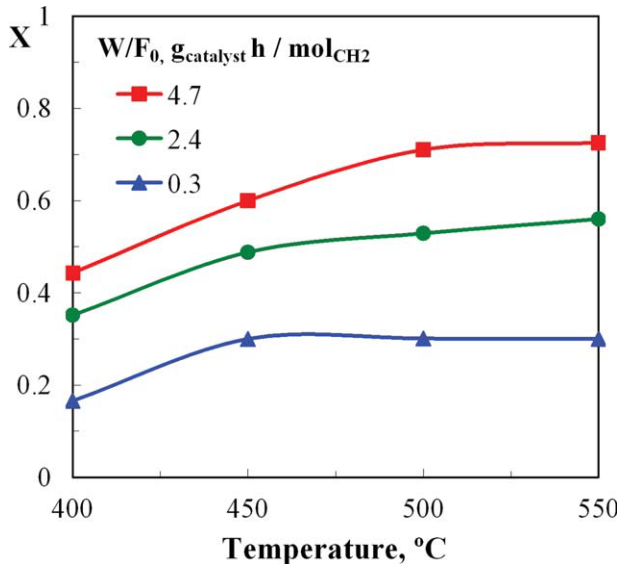

Figure 2. Effect of temperature on the apparent conversion of (methanol + dimethyl ether)/*n*-butane, for three values of space time.

[Color figure can be viewed in the online issue, which is available at wileyonlinelibrary.com.]

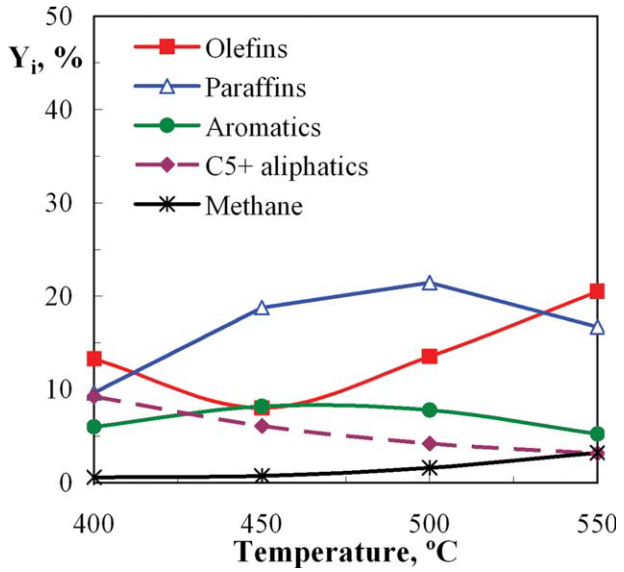

Figure 3. Effect of temperature on product yields for a space time of 2.4 (g of catalyst) h (mol CH_2)$^{-1}$.

[Color figure can be viewed in the online issue, which is available at wileyonlinelibrary.com.]

where F_0 and F_e are the molar flow rates of (methanol + dimethyl ether)/*n*-butane at the inlet and outlet, with both terms being expressed in CH_2 equivalent units.

Figure 3 shows the effect of temperature on the yields of the different lumps of products, for a space time of 2.4 (g of catalyst) h (mol CH_2)$^{-1}$. The yield of each lump has been calculated as

$$Y_i = \frac{F_i}{F_0} \tag{2}$$

where F_i is the molar flow rate of *i* lump in the product stream, being expressed in CH_2 equivalent units.

The effect of temperature on product distribution is qualitatively similar to that observed in the MTO process in this temperature range (Mier et al., submitted). The yield of C_2—C_4 olefins decreases as temperature is increased from 400 to 450°C, due to the enhancement of olefin oligomerization to higher-hydrocarbons. For temperatures higher than 450°C, the yield of olefins increases as temperature is increased, due to the cracking of hydrocarbons of higher-molecular weight. The enhancement in the yields of propylene and ethylene is more apparent by increasing temperature in the 450–550°C range (Figure 4).

Figure 5 shows the effect of space time on reaction product yields for 500°C. The rapid formation of C_2—C_4 olefins is observed, given that they are present in the reaction medium even from small values of space time. The yield of C_2—C_4 olefins peaks with space time for values ~0.5 (g of catalyst) h (mol CH_2)$^{-1}$ and tends asymptotically toward constant values, which are higher than those corresponding to thermodynamic equilibrium due to the limitation in the formation of hydrocarbons of high-molecular weight by the shape selectivity of HZSM-5 zeolite. Propylene is the major olefin (Figure 6) with a maximum yield of 7% for a space time of 1 (g of catalyst) h (mol CH_2)$^{-1}$.

This result is different to that observed in the MTO process, as the formation of olefins from methanol is activated by those formed in *n*-butane cracking. The maximum yield of olefins corresponds to higher-values of space time in the MTO process (Mier et al., submitted).

Paraffins, which are end products in the kinetic scheme, increase as space time is increased (Figure 5). Ethane is a

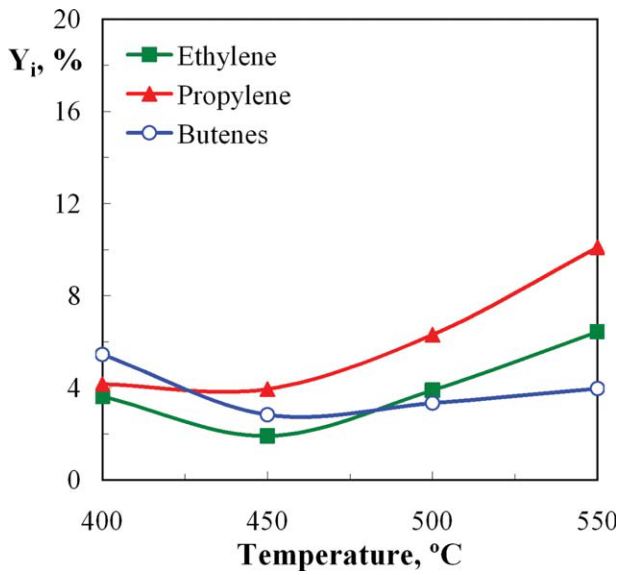

Figure 4. Effect of temperature on individual olefin yields for a space time of 2.4 (g of catalyst) h (mol CH_2)$^{-1}$.

[Color figure can be viewed in the online issue, which is available at wileyonlinelibrary.com.]

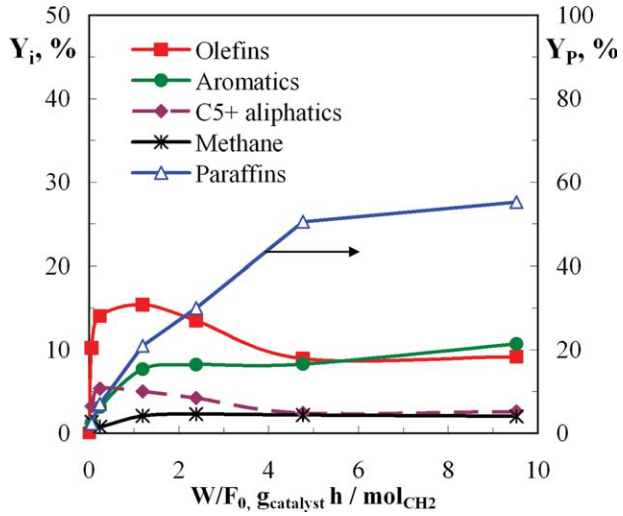

Figure 5. Effect of space time on product yields at 500°C.

[Color figure can be viewed in the online issue, which is available at wileyonlinelibrary.com.]

minor product in the whole operating condition range studied. For low-values of space time, isobutane is the major paraffin (80% of the paraffin lump), which is a similar amount to that corresponding to the MTO process (Mier et al., submitted). However, isobutane yield decreases to 10% for high-values of space time, with propane being the main paraffin (74% of paraffin lump), which is a similar result to that corresponding to *n*-butane cracking.[33]

The yield of C_{5+} aliphatic fraction peaks similarly as observed for C_2—C_4 olefins, due its prevailing content of C_{5+} olefins. The yield of this fraction, like that corresponding to aromatics and methane, tends to a constant pseudo-equilibrium value.

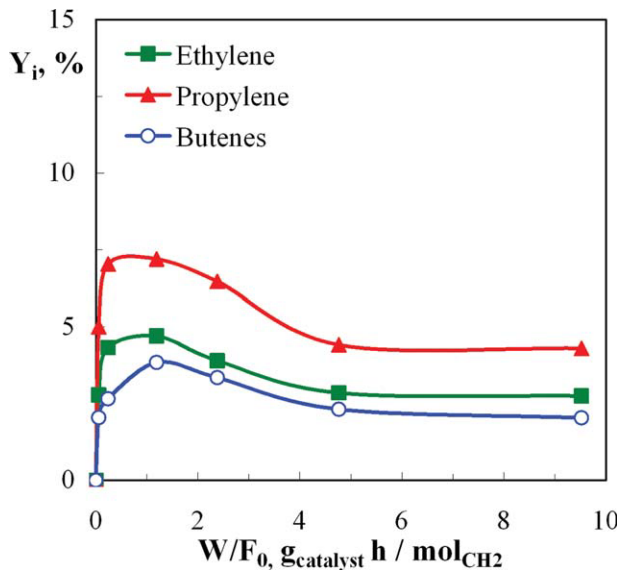

Figure 6. Effect of space time on individual olefin yield at 500°C.

[Color figure can be viewed in the online issue, which is available at wileyonlinelibrary.com.]

The effect of temperature and space time on catalyst deactivation is shown in Figures 7 and 8, where the evolution of product yields with time on stream is plotted for two different values of temperature (500°C in graphs a and 550°C in graphs b, respectively).

For a low-value of space time (results in Figure 7 corresponding to 0.06 (g of catalyst) h (mol CH_2)$^{-1}$), the yield of olefins is high at zero time on stream and catalyst deactivation is almost total for 1 h of time on stream affecting to all the product fraction. Similarly to *n*-butane cracking,[33] only the yield of paraffins and aromatics are affected by catalyst deactivation for higher-values of space time (Figure 8 corresponding to 9.5 (g of catalyst) h (mol CH_2)$^{-1}$), whereas the yield of the remaining reaction products remains almost constant for 5 h.

It should be noted that deactivation does not cause the unfavorable effect of increasing methane yield, which is lower than in the MTO process from zero time on stream,

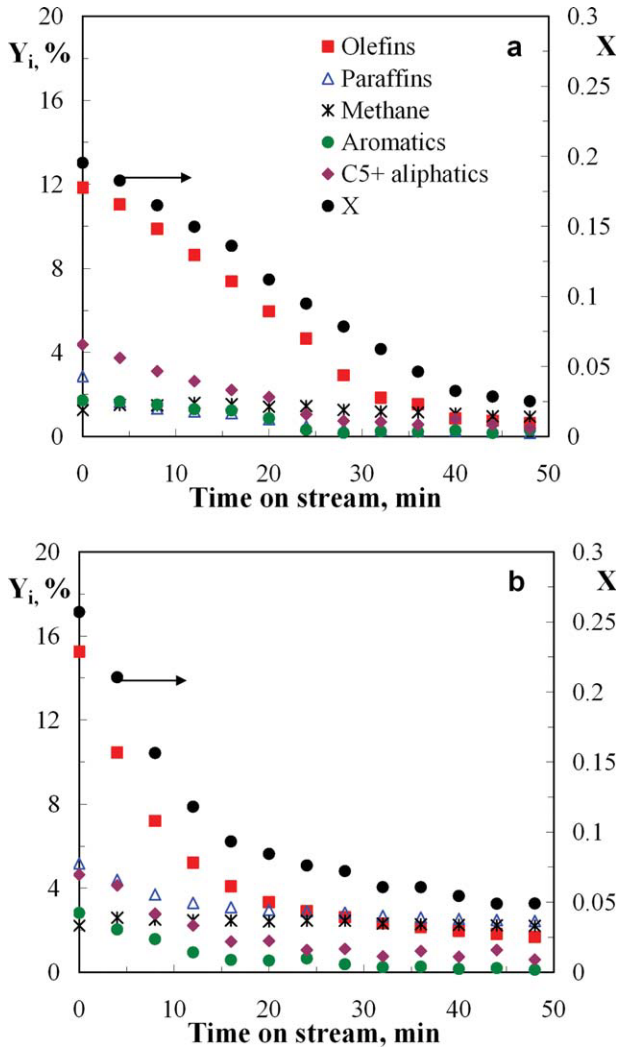

Figure 7. Evolution with time on stream of products yield, at 500°C (graph a) and 550°C (graph b), for a space time of 0.06 (g of catalyst) h (mol CH_2)$^{-1}$.

[Color figure can be viewed in the online issue, which is available at wileyonlinelibrary.com.]

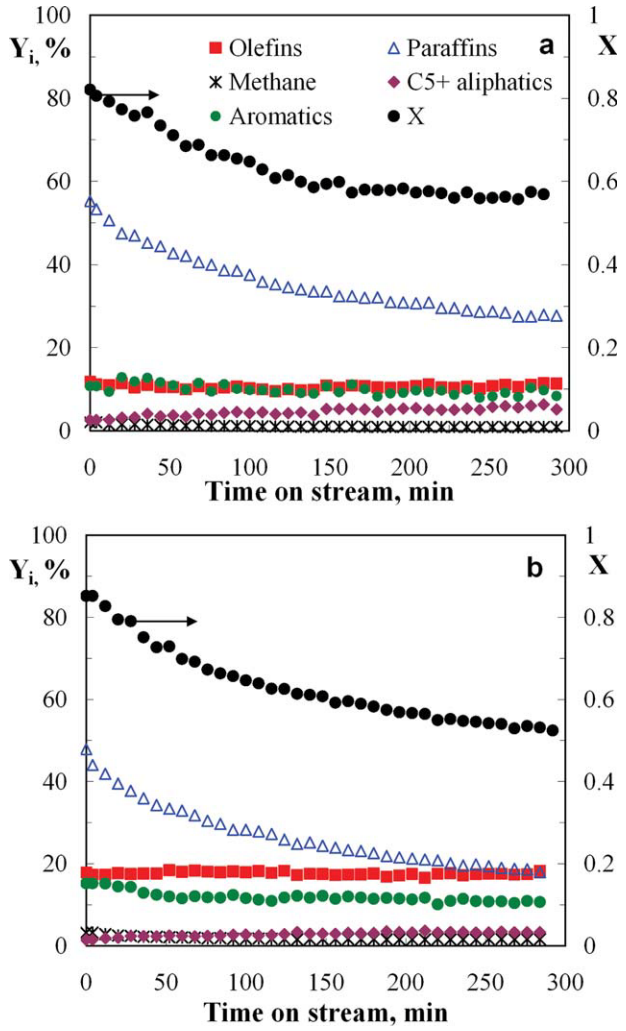

Figure 8. Evolution with time on stream of products yield, at 500°C (graph a) and 550°C (graph b), for a space time of 9.5 (g of catalyst) h (mol CH_2)$^{-1}$.

[Color figure can be viewed in the online issue, which is available at wileyonlinelibrary.com.]

where methane formation is favored by catalyst deactivation (Mier et al., submitted).[43]

Methodology for the kinetic study

Ideal flow (plug flow) has been assumed in the fixed-bed reactor, and isothermal regime has also been assumed, given that temperature differences at radial and longitudinal positions in the bed are lower than 1°C.

The reaction rate of each i compound at zero time on stream is calculated considering the different reaction steps in which this compound is involved.

$$r_i = \frac{dX_i}{d(W/F_0)} = \sum^{j} (\upsilon_i)_j r_j \tag{3}$$

where W is the mass of catalyst. X_i is the concentration of each lump expressed as the molar fraction by mass unit of organic compounds in the reaction medium, in CH_2 equivalent units. With this definition, the results of the integration of the kinetic equations correspond to concentration units that are easy to understand because of their physical meaning, being easy to relate to the yield and mass balance of the components (organics and inerts), y_i. $(\upsilon_i)_j$ is the stoichiometric coefficient of component i in the kinetic step j, and r_j is the reaction rate of the kinetic step j, with the concentration of each lump defined as the molar fraction by mass unit of reaction medium components (organics and inerts), y_i. Thus, these units for concentration are equal to partial pressure, p_i. This improves the physical meaning of concentration dependent terms in the kinetic equations by adapting them to a meaning that is consistent with the mass law. The empiricism of the kinetic equation is lower than when using the concentration-dependent term based on mass fractions, as is common practice (to simplify calculations) in catalytic reactions with complex reaction schemes.

The kinetic parameters for each kinetic model proposed have been calculated by multivariable nonlinear regression. Optimization has been carried out by minimizing an objective function established as the sum of squares of the differences between the experimental and calculated values of composition

$$\mathrm{OF} = \sum_{i=1}^{n_l} w_i \phi_i = \sum_{i=1}^{n_l} w_i \sum_{j=1}^{p} R_j \left(\overline{X}_{i,j}^{*} - X_{i,j} \right)^2 \tag{4}$$

where w_i is the weight factor for each lump i in the kinetic scheme; ϕ_i is the sum of squares for the lack of fit for each of these lumps, including the values obtained from the runs repeated under the same experimental conditions, R_j. Two runs are carried out for each combination of experimental conditions; $\overline{X}_{i,j}^{*}$ is the average experimental value of composition of each lump i determined from the experiments repeated under the same conditions j; $X_{i,j}$ is the corresponding value calculated integrating the mass balance for lump i, Eq. 3; n_l is the number of lumps in the kinetic scheme; and p is the total number of variable combinations used in the experimentation.

The kinetic parameters of best fit are the kinetic constants of each kinetic step j. To reduce the correlation between frequency factor and activation energy, the Arrhenius reparameterized equation has been used by expressing the kinetic constant, k_j, as a function of its correspondent value, k_j*, at a reference temperature, T*:[29–31]

$$k_j = k_j^{*} \exp\left[-\frac{E_j}{R} \left(\frac{1}{T} - \frac{1}{T^{*}} \right) \right] \tag{5}$$

The composition values of each lump for the proposed kinetic models have been calculated by integrating the expressions corresponding to Eq. 3, using a MATLAB program based on fourth-order finite-difference approximation. This program is combined with another one for multivariate nonlinear regression, also written in MATLAB, for calculating the kinetic parameters (kinetic constants for a reference temperature (500°C), k_j^{*}, and the corresponding activation energies, E_j). The nonlinear multivariable regression is performed by a MATLAB function, "fminsearch," which performs a detailed search of the optimum based on the SIMPLEX method.

The significance and discrimination of the proposed models has been carried out by using statistical criteria explained in detail elsewhere.[33]

Kinetic modeling for zero time on stream

Figure 9 shows the kinetic scheme corresponding to the best fit to the experimental results. The kinetic equations for the formation of each component or lump corresponding to this scheme are as follow

$$(r_{\mathrm{M}})_0 = -k_1 y_{\mathrm{M}}^2 + \left(\frac{k_1}{K} y_{\mathrm{D}} y_{\mathrm{W}}\right) - k_2 y_{\mathrm{M}} - k_5 y_{\mathrm{M}} - k_7 y_M y_{\mathrm{O}} \quad (6)$$

$$(r_D)_0 = k_1 y_{\mathrm{M}}^2 - \left(\frac{k_1}{K} y_{\mathrm{D}} y_{\mathrm{W}}\right) - k_3 y_{\mathrm{D}} - k_5 y_{\mathrm{D}} - k_8 y_{\mathrm{D}} y_{\mathrm{O}} \quad (7)$$

$$(r_{\mathrm{B}})_0 = k_{12} y_{\mathrm{O}}^2 - k_9 y_{\mathrm{B}} y_{\mathrm{O}} - (k_4 + k_6) y_{\mathrm{B}} \quad (8)$$

$$(r_{\mathrm{O}})_0 = k_2 y_{\mathrm{M}} + k_3 y_{\mathrm{D}} + k_4 y_{\mathrm{B}} + k_7 y_{\mathrm{M}} y_{\mathrm{O}} + k_8 y_{\mathrm{D}} y_{\mathrm{O}} + k_9 y_{\mathrm{B}} y_{\mathrm{O}} + k_{10} y_{\mathrm{P}} y_{\mathrm{O}} + k_{11} y_{\mathrm{G}} y_{\mathrm{O}} - (k_{12} + k_{13} + k_{14}) y_{\mathrm{O}}^2 \quad (9)$$

$$(\mathrm{r}_{\mathrm{P}})_0 = -k_{10} y_{\mathrm{P}} y_{\mathrm{O}} + k_{13} y_{\mathrm{O}}^2 \quad (10)$$

$$(r_{\mathrm{G}})_0 = -k_{11} y_{\mathrm{G}} y_{\mathrm{O}} + k_{14} y_{\mathrm{O}}^2 \quad (11)$$

$$(r_{\mathrm{C}})_0 = k_5 y_{\mathrm{M}} + k_5 y_{\mathrm{D}} + k_6 y_{\mathrm{B}} \quad (12)$$

It should be noted that all the hydrocarbons (C_{5+} aliphatics and aromatics) with more than five carbon atoms have been grouped into a single lump called C_5—C_{10} fraction (G). The steps in the kinetic scheme are:

Step 1: The dehydration of methanol to dimethyl ether and water, which is assumed to be in equilibrium and whose equilibrium constant, K, is related to temperature as follows:[29]

$$K = \exp\left[-9.76 + 3200\frac{1}{T} + 1.07\log T - 0.66 \cdot 10^{-3} T + 0.49 \cdot 10^{-7} T^2 + 6500\frac{1}{T^2}\right] \quad (13)$$

Steps 2–4: The formation of olefins from oxygenates (methanol and dimethyl ether) and *n*-butane.

Steps 5 and 6: The formation of methane by decomposition of oxygenates and *n*-butane.

Steps 7–11: Five autocatalytic stages to form olefins from the reaction of methanol, dimethyl ether, *n*-butane, paraffins, and C_5—C_{10} lump, respectively, with the olefins present in the reaction medium.

Steps 12–14: The formation of *n*-butane, paraffins, and C_5—C_{10} lump from olefins.

The differences with the kinetic scheme proposed for the MTO process in the 400–550°C (Mier et al., submitted), range are: (i) the consideration of two stages, 4 and 6, characteristics of the kinetic scheme of *n*-butane transformation into olefins and methane;[33] (ii) Step 9, which considers the reaction of *n*-butane with olefins.

The calculated kinetic parameters, the objective function, and the statistic parameters for the kinetic model are set out in Table 2. The adequacy of fit is shown in Figure 10, where

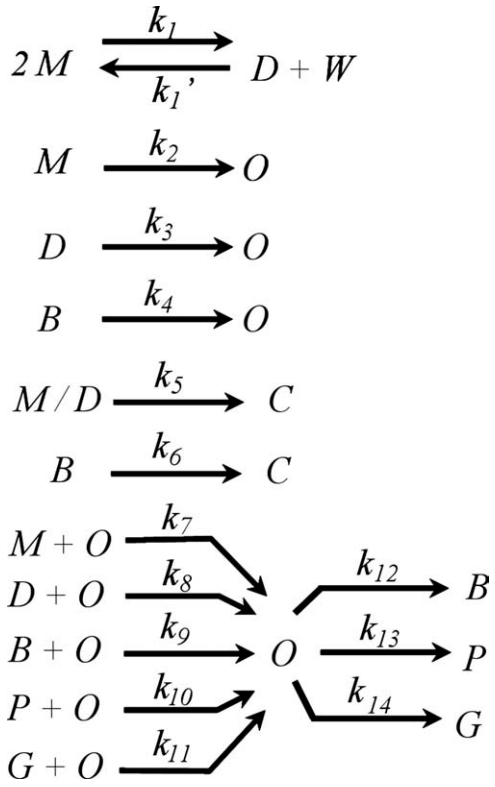

Figure 9. Kinetic scheme proposed for the joint transformation of methanol and *n*-butane.

the experimental results (points) of lump composition are compared with those calculated using the kinetic model (lines) for different values of space time at zero time on stream for three values of temperature. The regression coefficient corresponding to the fit is $R^2 = 0.97$.

When comparing the kinetic parameters determined for the integrated process with the parameters corresponding to the same reaction steps in the individual processes (cracking of *n*-butane and methanol transformation into olefins) (Mier et al., submitted)[33], it should be noted that the kinetic model for the integrated process is not a linear combination of the corresponding individual processes. Consequently, although it is able to predict the results for the integrated process, it does not fit the results for the individual ones. A comparison of the kinetic parameters obtained using the same catalyst and in the same operating condition range leads to the following remarks:

The kinetic constant for the formation of olefins from *n*-butane is an order of magnitude higher in the integrated process than in the cracking of *n*-butane,[33] and much higher than that for the formation of olefins from methanol (due to the initiation steps) (Mier et al., submitted). This is a consequence of the aforementioned synergy.

The kinetic constant for *n*-butane formation from olefins is very high in the integrated process, high in the transformation of methanol (Mier et al., submitted) and insignificant in the cracking of *n*-butane.[33]

Table 2. Kinetic Parameters of Best Fit, Objective Function, and Variance Analysis for the Kinetic Model

Kinetic Parameters	
k_1^* [$mol_{CH_2}\ g_{catal}^{-1}\ h^{-1}(mol_M/mol)^{-2}$]	24.5
k_2^* [$mol_{CH_2}\ g_{catal}^{-1}\ h^{-1}(mol_M/mol)^{-1}$]	$1.1 \times \cdot 10^{-5}$
k_3^* [$mol_{CH_2}\ g_{catal}^{-1}\ h^{-1}(mol_D/mol)^{-1}$]	$1.7 \times \cdot 10^{-5}$
k_4^* [$mol_{CH_2}\ g_{catal}^{-1}\ h^{-1}(mol_B/mol)^{-1}$]	3.94
k_5^* [$mol_{CH_2}\ g_{catal}^{-1}\ h^{-1}(mol_C/mol)^{-1}$]	0.202
k_6^* [$mol_{CH_2}\ g_{catal}^{-1}\ h^{-1}(mol_B/mol)^{-1}$]	0.014
k_7^* [$mol_{CH_2}\ g_{catal}^{-1}\ h^{-1}(mol_M mol_O/mol^2)^{-1}$]	91.4
k_8^* [$mol_{CH_2}\ g_{catal}^{-1}\ h^{-1}(mol_D mol_O/mol^2)^{-1}$]	283
k_9^* [$mol_{CH_2}\ g_{catal}^{-1}\ h^{-1}(mol_B mol_O/mol^2)^{-1}$]	0.124
k_{10}^* [$mol_{CH_2}\ g_{catal}^{-1}\ h^{-1}(mol_P mol_O/mol^2)^{-1}$]	1.65
k_{11}^* [$mol_{CH_2}\ g_{catal}^{-1}\ h^{-1}(mol_G mol_O/mol^2)^{-1}$]	84.7
k_{12}^* [$mol_{CH_2}\ g_{catal}^{-1}\ h^{-1}(mol_O/mol)^{-2}$]	109
k_{13}^* [$mol_{CH_2}\ g_{catal}^{-1}\ h^{-1}(mol_O/mol)^{-2}$]	20.4
k_{14}^* [$mol_{CH_2}\ g_{catal}^{-1}\ h^{-1}(mol_O/mol)^{-2}$]	39.2
E_1 (kJ mol^{-1})	54.4
E_2 (kJ mol^{-1})	4.35
E_3 (kJ mol^{-1})	187
E_4 (kJ mol^{-1})	49.4
E_5 (kJ mol^{-1})	107
E_6 (kJ mol^{-1})	86.2
E_7 (kJ mol^{-1})	4.27
E_8 (kJ mol^{-1})	55.7
E_9 (kJ mol^{-1})	65.7
E_{10} (kJ mol^{-1})	177
E_{11} (kJ mol^{-1})	48.1
E_{12} (kJ mol^{-1})	4.68
E_{13} (kJ mol^{-1})	4.26
E_{14} (kJ mol^{-1})	5.02
OF	0.912
ϕ_f	0.406
v_f	110
s_f^2	3.7×10^{-3}
ϕ_e	0.061
v_e	28
s_e^2	2.2×10^{-3}
s_f^2/s_e^2	1.68
$F_{0.05}$ (v_f,v_e)	1.71
Significance test	Valid

The kinetic constant for paraffin formation from olefins is higher in the cracking of *n*-butane compared with the other two processes. This is explained because the presence of water in the reaction medium attenuates hydrogen transfer reactions.

The gasoline formation step is very important in methanol transformation (Mier et al., submitted) and the kinetic constant is an order of magnitude higher than that for *n*-butane cracking.[33] This result is link to the high-concentration of light olefins as primary products that are exclusive to methanol transformation.

The kinetic constants corresponding to the reaction steps of *n*-butane and paraffins with olefins to form more olefins have much higher-values in methanol transformation (Mier et al., submitted). This result is consistent with the higher-concentration of olefins than in the integrated process and *n*-butane transformation.[33]

Consideration of deactivation in the kinetic model

The "past history" of the catalyst (deactivation) at each longitudinal position in the reactor has been considered by incorporating an activity term, *a*, in Eq. 3

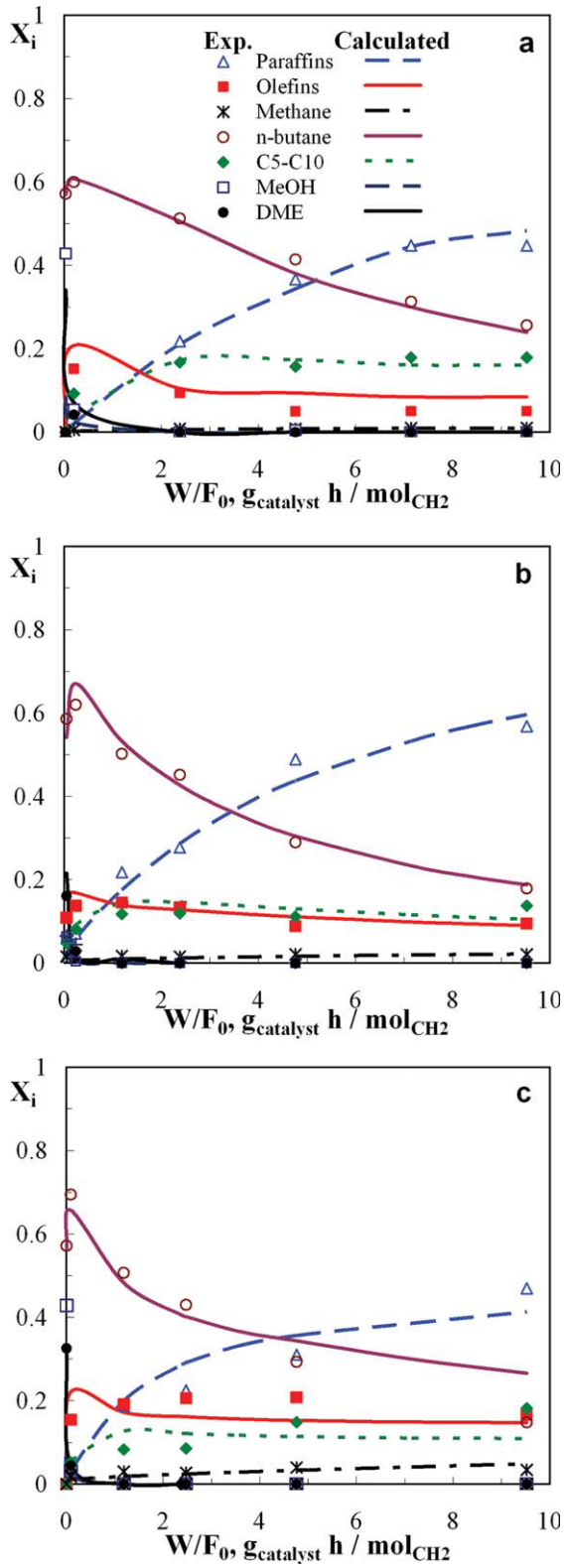

Figure 10. Comparison of experimental (points) and calculated (lines) values for the evolution of product composition with space time at zero time on stream.

Graph a, 450°C. Graph b, 500°C. Graph c, 550°C. [Color figure can be viewed in the online issue, which is available at wileyonlinelibrary.com.]

Table 3. Effect of Space Time on Coke Content Deposited on the Catalyst after 5 h Time on Stream, at 450 and 500°C

	Coke Content, wt%	
Space time (g catalyst) [h (mol CH_2)$^{-1}$]	450°C	500°C
0.24	4.6	6.7
1.19	4.3	6.4
2.38	4.1	4.5
7.14	2.5	3.4

$$r_i = \sum^{j} (\upsilon_i)_j \mathrm{r}_j a \tag{14}$$

Activity, a, is defined as the ratio between the reaction rate at t time on stream and zero time on stream

$$a = \frac{r_i}{(r_i)_{t=0}} \tag{15}$$

Given that the different steps in the kinetic scheme are not uniformly affected by deactivation, a selective kinetic model of deactivation has been considered.

Consequently, the same deactivation rate has been considered for all the steps in the kinetic scheme, with the exception of: (i) methanol dehydration to dimethyl ether (Step 1), for which the activity has been considered constant and equal to unity, given that no deactivation is observed in any experimental condition studied; (ii) methane formation from oxygenates and *n*-butane (Steps 5 and 6). Methane concentration does not decrease steadily with time on stream as do the remaining lumps of products in the kinetic scheme, but methane yield increases with time on stream under certain conditions (particularly for low-values of space time). This result leads to the conclusion that deactivation in methane formation is slower than in the remaining steps in the kinetic scheme, with this behavior being quantified as activity a_C, which to simplify the kinetic scheme has been calculated by relating it to the activity of the other steps, a, with a constant exponent, m, according to the following expression

$$a_C = a^m \tag{16}$$

The fact that methanol dehydration is not affected by catalyst deactivation by coke deposition is because this step requires few and weak acid sites. Furthermore, the need for a different activity for quantifying the increase in methane formation with time on stream is explained because reactant decomposition occurs mainly by thermal degradation and, consequently, catalyst deterioration is less than in exclusively catalytic steps.

The kinetic equations for the formation of product lumps for any value of time on stream, by considering activities a and a_C, are as follow

$$(r_M)_t = -k_1 y_M^2 + \left(\frac{k_1}{K} y_D y_W\right) - (k_2 y_M + k_7 y_M y_O)\, a - (k_5 y_M) a^m \tag{17}$$

$$(r_D)_t = k_1 y_M^2 - \left(\frac{k_1}{K} y_D y_W\right) - (k_3 y_D + k_8 y_D y_O)\, a - (k_5 y_D) a^m \tag{18}$$

$$(r_B)_t = (-k_4 y_B - k_9 y_B y_O + k_{12} y_O^2)\, a - (k_6 y_B) a^m \tag{19}$$

$$(\mathrm{r_O})_t = (k_2 y_M + k_3 y_D + k_4 y_B + k_7 y_M y_O + k_8 y_D y_O + k_9 y_B y_O + k_{10} y_P y_O + k_{11} y_G y_O - (k_{12} + k_{13} + k_{14}) y_O^2) a \tag{20}$$

$$(r_P)_t = (-k_{10} y_P y_O + k_{13} y_O^2) a \tag{21}$$

$$(r_G)_t = (-k_{11} y_G y_O + k_{14} y_O^2) a \tag{22}$$

$$(r_C)_t = (k_5 y_M + k_5 y_D + k_6 y_B)\ \mathrm{a^m} \tag{23}$$

Previous studies on the transformation of methanol on HZSM-5 zeolite catalysts have been taken into account to establish the kinetic equation of deactivation. Equations dependent on the concentration of reaction components have been proposed in the literature by considering that oxygenates are the main coke precursors, although this formation is also favored by the concentration of C_2—C_4 olefins and C_{5+} lump.[15,43,44] Coke formation from oxygenates is explained through the ''hydrocarbon pool'' mechanism,[26,27,45,46] and coke formation mechanism on HZSM-5 zeolites from olefins and aromatics, which are well-established in the literature.[35,47]

The results of coke content deposited on the catalyst for different values of space time at 450 and 500°C (Table 3) reveal that coke deposition is favored by higher-concentrations of oxygenates in the reaction medium (corresponding to a lower-space time). These results are similar to those obtained in methanol transformation.[48,49] For a value of space time of 2.3 (g of catalyst) h (mol CH_2)$^{-1}$ at 550°C and for 5 h of time on stream, the surface area of the deactivated catalyst is 149 $m^2\ g^{-1}$, (220 $m^2\ g^{-1}$ for fresh catalyst), which is a consequence of a decrease in micropore volume (0.044 $cm^3\ g^{-1}$ for fresh catalyst and 0.022 $cm^3\ g^{-1}$ for deactivated catalyst). Based on the results of temperature programmed oxidation (TPO) of the coke, it is mainly deposited on the micropores of the HZSM-5 zeolite.

The following equation has been established by discriminating different models dependent on the concentration of lumps in the reaction medium

$$\frac{da}{dt} = -[k_{d1}(y_M + y_D)\ + k_{d2}(y_O + y_G)]\, a \tag{24}$$

This equation considers that deactivation is dependent on the concentration of the lumps of oxygenates, C_2—C_4 olefins and C_5—C_{10} fraction. The different models assayed are empirical expressions that consider the formation of coke depending on the concentration of reactants (in parallel), products (in series), and reactants and products (series–parallel).[50]

The methodology for calculating the kinetic parameters is similar to that explained in Methodology for the kinetic

Table 4. Kinetic Parameters of Best Fit and Objective Function for the Kinetic Model of the Deactivation

Kinetic Parameters	
k^*_{d1} (h^{-1})	$5.46 \cdot 10^{-2}$
k^*_{d2} (h^{-1})	$4.16 \cdot 10^{-2}$
E_{d1} (J mol^{-1})	50.2
E_{d2} (J mol^{-1})	44.8
m	0.12
OF	15.499

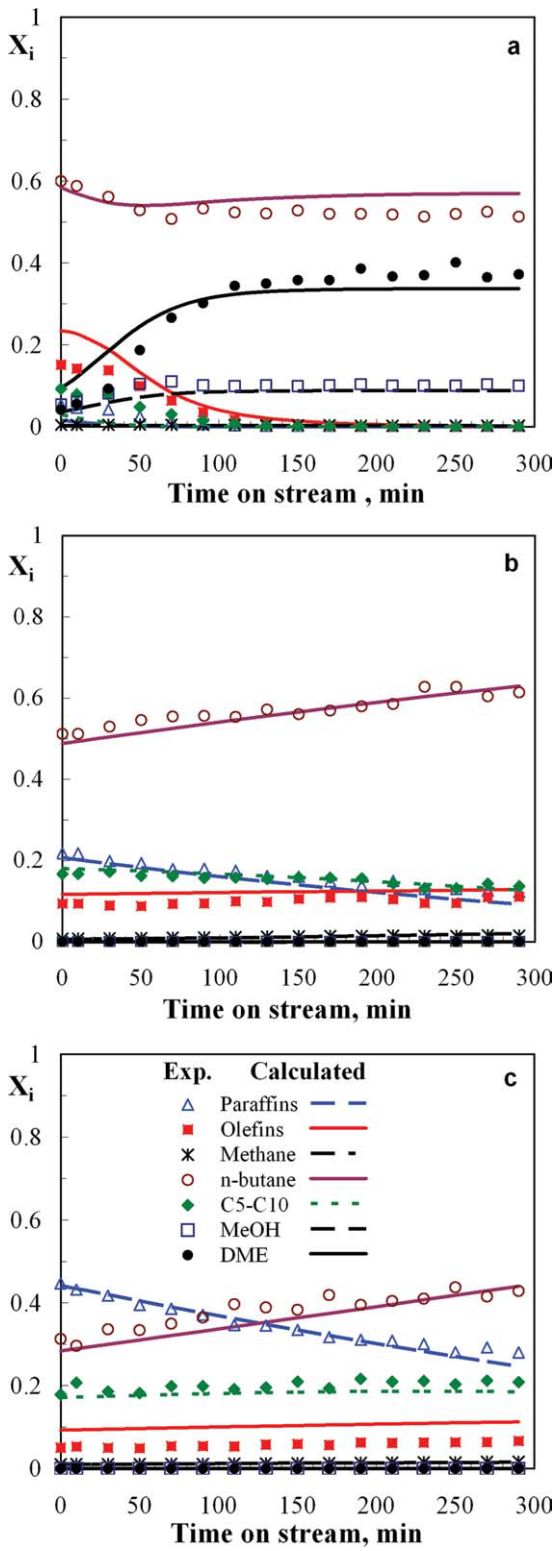

Figure 11. Comparison of experimental (points) and calculated (lines) values for the evolution of product composition with time on stream, at 450°C.

Graph a, space time, 0.143 (g of catalyst) h (mol CH_2)$^{-1}$. Graph b, 2.4 (g of catalyst) h (mol CH_2)$^{-1}$. Graph c, 7.14 (g of catalyst) h (mol CH_2)$^{-1}$. [Color figure can be viewed in the online issue, which is available at wileyonlinelibrary.com.]

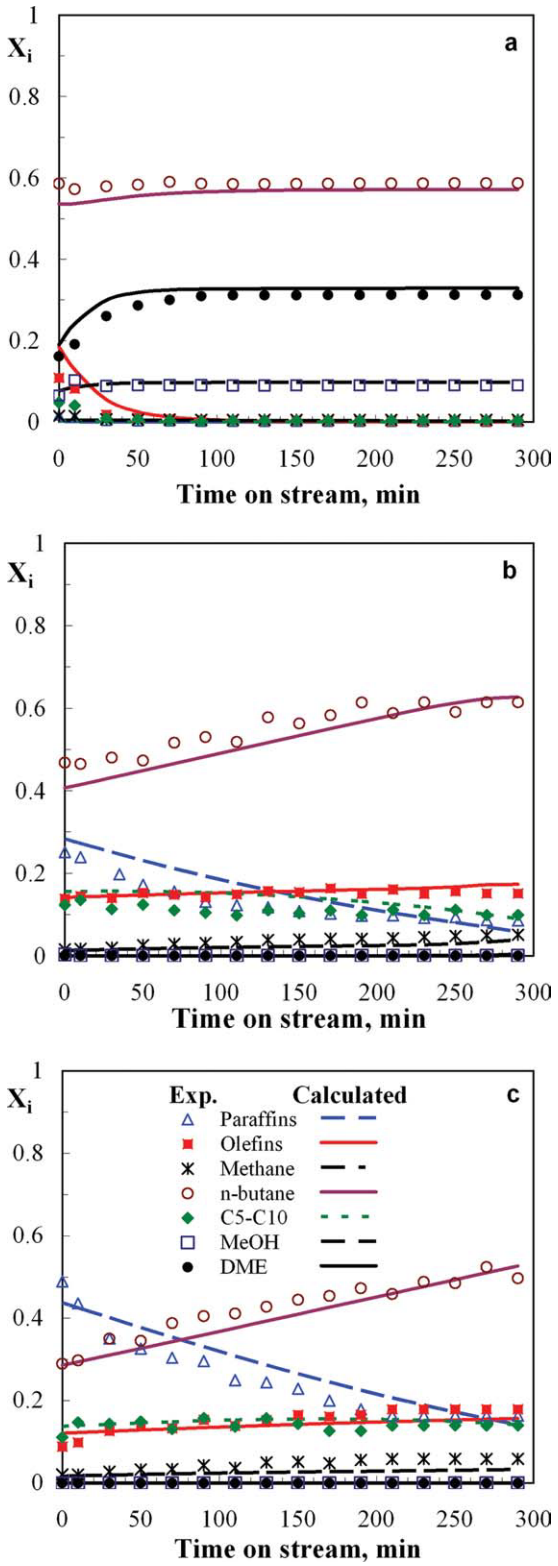

Figure 12. Comparison of experimental (points) and calculated (lines) values for the evolution of product composition with time on stream, at 500°C.

Graph a, space time, 0.06 (g of catalyst) h (mol CH_2)$^{-1}$. Graph b, 2.4 (g of catalyst) h (mol CH_2)$^{-1}$. Graph c, 4.7 (g of catalyst) h (mol CH_2)$^{-1}$. [Color figure can be viewed in the online issue, which is available at wileyonlinelibrary.com.]

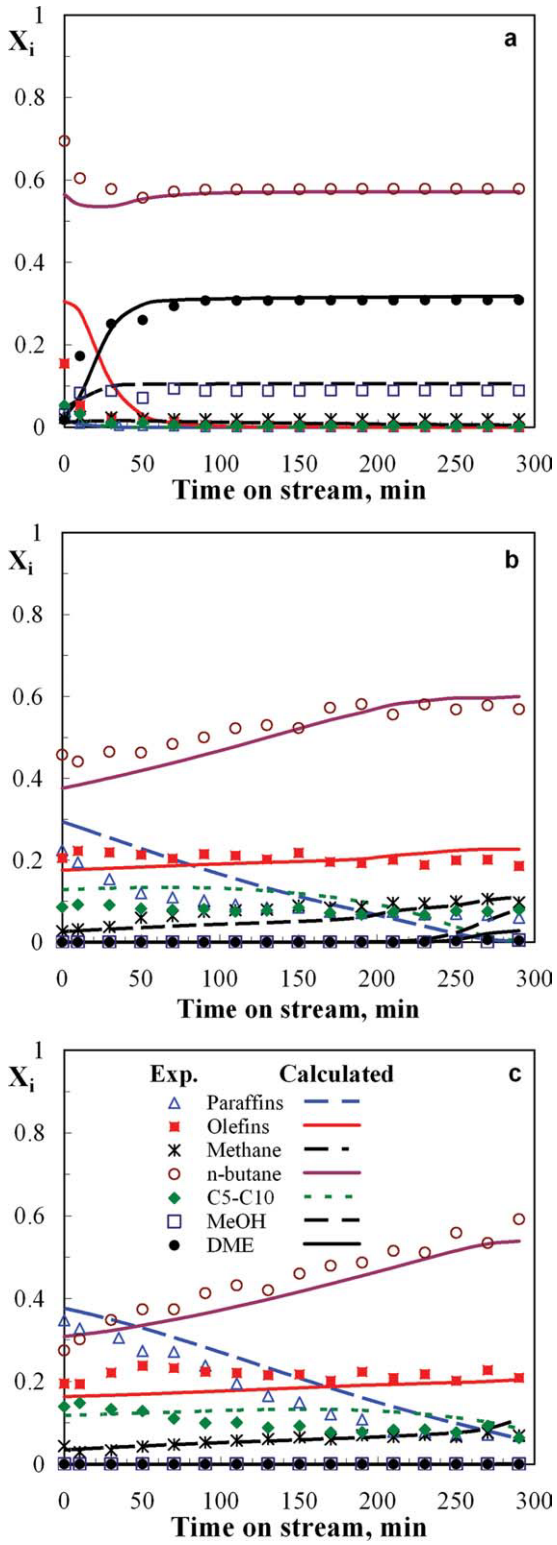

Figure 13. Comparison of experimental (points) and calculated (lines) values for the evolution of product composition with time on stream, at 550°C.

Graph a, space time, 0.06 (g of catalyst) h (mol CH_2)$^{-1}$. Graph b, 2.4 (g of catalyst) h (mol CH_2)$^{-1}$. Graph c, 4.7 (g of catalyst) h (mol CH_2)$^{-1}$. [Color figure can be viewed in the online issue, which is available at wileyonlinelibrary.com.]

study section for the kinetics at zero time on stream. Equations 17–23 are integrated together with the kinetic equations of deactivation, Eqs. 16 and 24 to obtain the calculated values of concentration for product lumps. Given that the result of optimization strongly depends on the starting point, and to reduce the number of parameters to be optimized and make the search for the optimum easier, the kinetic constants determined at zero time on stream (Table 2) have been used in the calculation with a program written in MATLAB. The discrimination between possible deactivation kinetic models has been carried out based on the one hand on significance tests for the lack of fit of each model, by comparing this lack with the experimental error obtained by the repeated runs, and on the other, on significance tests between models to check whether one model is significantly better than another one.[33]

The kinetic parameters of best fit are set out in Table 4. A comparison of k_{d1} and k_{d2} values at 500°C shows that the term dependent on oxygenate concentration in Eq. 24 is more significant than the term dependent on olefin and C_5—C_{10} lump concentrations. Moreover, the term $m = 0.12$ in Eq. 16 shows that the formation of methane is hardly affected by catalyst deactivation.

The adequacy of fit is shown in Figures 11–13, where the experimental results (points) of lump composition with time on stream are compared with those calculated using the kinetic model (lines). Each graph corresponds to a different temperature (450, 500, and 550°C) and to a specific value of space time. The regression coefficient corresponding to the fit is $R^2 = 0.96$.

Conclusions

The cofeeding of methanol and paraffins (*n*-butane in this work) into the same reactor with a HZSM-5 zeolite catalyst is interesting for working under energy neutral conditions. Moreover, synergies of special interest take place in the integrated process for the production of C_2—C_4 olefins.

The presence of C_2—C_4 olefins produced by *n*-butane cracking in the reaction medium from low-values of space time activates the formation of the intermediates for methanol transformation, which is relevant for transforming methanol with low-values of space time. The integrated process accelerates the autocatalytic "hydrocarbon pool" mechanism characteristic to the MTO process.

Olefin yield increases as temperature is increased above 450°C, due to the cracking of higher-hydrocarbons, with the increase in propylene being almost linear with temperature. This strategy is more feasible than in the MTO process, as the unfavorable effects of methane, CO, and CO_2 formation are attenuated.

The results of product distribution show that the characteristics of the MTO process prevail for low-values of space time, whereas the characteristics of *n*-butane cracking prevail for high-values of space time. The kinetic scheme proposed uses steps from the kinetic schemes of both individual reactions, quantifying synergies between them.

The deactivation of the integrated process has its origin in coke deposition and is notably slower than that of the MTO process in the same temperature range studied. A kinetic model of deactivation has been determined, considering that

methanol dehydration has an insignificant deactivation and that the formation of methane has a partially catalytic origin. The deactivation equation shows that oxygenates are the main coke precursors, although this coke is also partially formed by the degradation of C_2—C_4 olefins and C_5—C_{10} lumps.

The kinetic model allows quantifying the product distribution of reaction medium components (methanol, dimethyl ether, *n*-butane, C_2—C_4 paraffins, C_2—C_4 olefins, and C_5—C_{10} lump) in a wide range of conditions (between 400 and 550°C, up to 9.5 (g of catalyst) h (mol CH_2)$^{-1}$ and with a time on stream of 5 h), and will be a tool of great interest for future studies aimed at process scaling-up.

Acknowledgments

This work was carried out with the financial support of the Department of Education, Universities, and Research of the Basque Government (Project GIC07/24-IT-220-07) and of the Ministry of Science and Innovation of the Spanish Government (Project CTQ2007-66571/PPQ).

Notation

a, a_C = activities defined as a ratio of reaction rates, Eqs. 15 and 16
B, C, D, G, O, P, M, W = *n*-butane, methane, dimethyl ether, C_5—C_{10} lump, C_2—C_4 olefins, C_2—C_4 paraffins without *n*-butane, methanol and water, respectively
d_p = pore diameter, Å
E_j = activation energy for each kinetic constant, kJ mol^{-1}
F_0, F_e = molar flow rate of oxygenates + *n*-butane at the inlet and outlet of the reactor, respectively, CH_2 equivalent units (mol h^{-1})
F_i = molar flow rate of *i* component in the output stream, CH_2 equivalent units (mol h^{-1})
K = thermodynamic equilibrium constant in the methanol transformation process
k_j, k_j^* = constants of step *j* at any temperature and that corresponding to the reference temperature, units are those corresponding to the kinetic equation
m = constant, Eq. 16
n_1 = number of lumps
OF = error objective function, Eq. 4
p = number of variable combinations studied
R = universal gas constant, kJ (mol K)$^{-1}$
r_i = reaction rate of component *i* at zero time on stream, $(mol_i)_{CH2}$ (g of catalyst h)$^{-1}$
r_j = reaction rate equation of step *j* in the kinetic scheme
R_j = number of repetitions under given experimental conditions
S_{BET} = BET surface area, m^2 g^{-1}
T, T^* = temperature and reference temperature, K
V_m, V_p = micropore and pore volume, cm^3 g^{-1}
W = catalyst mass, g
X = apparent conversion of (methanol + dimethyl ether)/*n*-butane, Eq. 1
w_i = weight factor for each lump *i*
X_i = molar fraction of lump *i* by mass unit of organic compounds, in CH_2 equivalent units
$X_{i,j}$, $\overline{X}^*_{i,j}$ = calculated value of each *i* lump composition for the experimental condition *j*, and average value determined with experiments repeated under the same experimental combination *j*, in CH_2 equivalent units
y_i = molar fraction of lump *i*, by mass unit of all the components in the reaction medium
Y_i = yield of *i* component, Eq. 2

Greek letters

ϕ_f, ϕ_e = sum of squares for the lack of fit and for pure experimental error
ν_f, ν_e = degrees of freedom for the lack of fit and of pure experimental error
$(\upsilon_i)_j$ = stoichiometric coefficient of component *i* in step *j* in the kinetic scheme

Literature Cited

1. Martin A, Nowak S, Lücke B, Günschel H. Coupled conversion of methanol and C_4 hydrocarbons to lower olefins. *Appl Catal*. 1989;50:149–155.
2. Martin A, Nowak S, Lücke B, Wieker W, Fahlke B. Coupled conversion of methanol and C_4-hydrocarbons (CMHC) on iron-containing ZSM-5 type zeolites. *Appl Catal*. 1990;57:203–214.
3. Lücke B, Martin A, Günschel H, Nowak S. CMHC: coupled methanol hydrocarbon cracking—Formation of lower olefins from methanol and hydrocarbons over modified zeolites. *Microp Mesop Mater*. 1999;29:145–157.
4. Yin X, Leung DYC. Characteristics of the synthesis of methanol using biomass-derived syngas. *Energy Fuels*. 2005;19:305–310.
5. Ren T, Patel M, Blok K. Olefins from conventional and heavy feedstocks: energy use in steam cracking and alternative processes. *Energy*. 2006;31:425–451.
6. Ren T, Patel M, Blok K. Steam cracking and methane to olefins: energy use, CO_2 emissions and production costs. *Energy*. 2008;33:817–833.
7. Guisnet M, Gnep NS, Aittaleb D, Doyement YJ. Conversion of light alkanes into aromatic hydrocarbons: VI. Aromatization of C_2-C_4 alkanes on H-ZSM-5 -Reaction mechanisms. *Appl Catal A Gen*. 1992;87:255–270.
8. Shertukde PV, Marcelin G, Sill GA, Hall WK. Study of the mechanism of the cracking of small alkane molecules on HY zeolites. *J Catal*. 1991;136:446–462.
9. Wang X, Zhao Z, Xu Ch, Duan A, Zhang L, Jiang G. Effects of light rare earth on acidity and catalytic performance of HZSM-5 zeolite for catalytic cracking of butane to light olefins. *J Rare Earths*. 2007;25:321–328.
10. Chang CD. Methanol conversion to light olefins. *Catal Rev-Sci Eng*. 1984;26:323–345.
11. Gayubo AG, Aguayo AT, Olazar M, Vivanco R, Bilbao J. Kinetics of the irreversible deactivation of the HZSM-5 catalyst in the MTO process. *Chem Eng Sci*. 200;58:5239–5249.
12. Kaarsholm M, Joensen F, Nerlov J, Cenni R, Chaouki J, Patience GS. Phosphorus modified ZSM-5: deactivation and product distribution for MTO. *Chem Eng Sci*. 2007;62:5527–5532.
13. Chen JQ, Bozzano A, Glover B, Fuglerud T, Kvisle S. Recent advancements in ethylene and propylene production using the UOP/Hydro MTO process. *Catal Today* 2005;106:103–107.
14. Aguayo AT, Gayubo AG, Vivanco R, Olazar M, Bilbao J. Role of acidity and microporous structure in alternative catalysts for the transformation of methanol into olefins. *Appl Catal A Gen*. 2005;283:197–207.
15. Gayubo AG, Aguayo AT, Castilla M, Olazar M, Bilbao J. Consideration of the role of water in the kinetic modelling of HZSM-5 zeolite deactivation by coke in the transformation of methanol into hydrocarbons. *AIChE J*. 2002;48:1561–1571.
16. Gayubo AG, Aguayo AT, Atutxa A, Prieto R, Bilbao J. Deactivation of a HZSM-5 catalyst in the transformation of the aqueous fraction of biomass pyrolysis-oil into hydrocarbons. *Energy Fuels*. 2004;18:1640–1647.
17. Martin A, Nowak S, Lücke B, Wieker W, Fahlke B. Iron-containing ZSM-5 type zeolites used in the coupled methanol-hydrocarbon cracking. *Stud Surf Sci Catal*. 1991;65:315–325.
18. Benito PL, Aguayo AT, Gayubo AG, Bilbao J. Hydrocarbons by reaction-regeneration cycles. *Ind Eng Chem Res*. 1996;35:2177–2182.
19. Mier D, Aguayo AT, Gayubo AG, Olazar M, Bilbao J. Catalyst discrimination for olefin production by coupled methanol/n-Butane cracking. *Appl Catal A: General*. 2010;383:202–210.

20. Mier D, Aguayo AT, Gayubo AG, Olazar M, Bilbao J. Synergies in the production of olefins by combined cracking of n-butane and methanol on a HZSM-5 zeolite catalyst. *Chem Eng J*. 2010;160: 760–769.
21. Dahl IM, Kolboe S. On the reaction mechanism for propene formation in the MTO reaction over SAPO-34. *Catal Lett*. 1993;20:329–336.
22. Dahl IM, Kolboe S. On the reaction mechanism for hydrocarbon formation from methanol over SAPO-34. 1. Isotopic labeling studies of the co-reaction of ethene and methanol. *J Catal*. 1994;149:458–464.
23. Svelle S, Joensen F, Nerlov J, Olsbye U, Lillerud KP, Kolboe S, Bjorgen M. Conversion of methanol into hydrocarbons over zeolite HZSM-5: ethene formation is mechanistically separated from the formation of higher alkenes. *J Am Chem Soc*. 2006;128:14770–14771.
24. Svelle S, Kolboe S, Swing O, Olsbye U. Methylation of alkenes and methylbenzenes by dimethyl ether or methanol on acidic zeolites. *J Phys Chem B*. 2005;109:12874–12878.
25. Svelle S, Ronning PO, Olsbye U, Kolboe S. Kinetic studies of zeolite-catalyzed methylation reactions. Part 2. Co-reaction of [^{12}C]propene or [^{12}C]*n*-butene and [^{13}C]methanol. *J Catal*. 2005;234:385–400.
26. Jiang Y, Huang J, Reddy Marthala VR, Ooi YS, Weitkamp J, Hunger M. In situ MAS NMR/UV/Vis investigation of H-SAPO-34 catalysts partially coked in the methanol-to-olefin conversion under continuous-flow conditions and their regeneration. *Microp Mesop Mater*. 2007;105:132–139.
27. Hereijgers BPC, Bleken F, Nilsen MH, Svelle S, Lillerud KP, Bjorgen M, Weckhuysen BM, Olsbye U. Product shape selectivity dominates the methanol-to olefins (MTO) reaction over a H-SAPO-34 catalysts. *J Catal*. 2009;264:77–87.
28. Aguayo AT, Gayubo AG, Ortega JM, Olazar M, Bilbao J. Catalyst deactivation by coke in the MTG process in fixed and fluidized beds reactors. *Catal Today*. 1997;37:239–248.
29. Gayubo AG, Aguayo AT, Alonso A, Bilbao J. Kinetic modeling of the methanol-to-olefins process on a silicoaluminophosphate (SAPO-18) catalyst by considering deactivation and the formation of individual olefins. *Ind Eng Chem Res*. 2007;46:1981–1989.
30. Castaño P, Arandes JM, Pawelec B, Olazar M, Bilbao J. Kinetic modelling for assessing product distribution in toluene hydrocracking on a Pt/HZM-5 catalyst. *Ind Eng Chem Res*. 2008;47:1043–1050.
31. Castaño P, Gutiérrez A, Villanueva I, Pawelec B, Bilbao J, Arandes JM. Effect of the support acidity on the aromatic ring-opening of pyrolysis gasoline over Pt/HZSM-5 catalysts. *Catal Today*. 2009; 143:115–119.
32. Chang F, Wei Y, Liu X, Qi Y, Zhang D, He Y, Liu Z. An improved catalytic cracking of n-hexane *via* methanol coupling reaction over HZSM-5 zeolite catalysts. *Catal Lett*. 2006;106:171–176.
33. Mier D, Aguayo AT, Gamero M, Gayubo AG, Bilbao J. Kinetic modelling of n-butane cracking on HZSM-5 zeolite. *Ind Eng Chem*. 2010;49:8415–8423.
34. Mier D, Aguayo AT, Gayubo AG, Gamero M, Bilbao J. Kinetics of methanol transformation into hydrocarbons over HZSM-5 zeolite catalyst at high temperature (400–550°C). *Ind Eng Chem*. 2010, accepted.
35. Guisnet M, Costa L, Ramôa Ribeiro F. Prevention of zeolite deactivation by coking. *J Mol Catal A Chem*. 2009;305:69–83.
36. Kim J, Choi M, Ryoo R. Effect of mesoporosity against the deactivation of MFI zeolite catalyst during the methanol-to-hydrocarbon conversion process. *J Catal*. 2010;269:219–228.
37. Ortega JM, Gayubo AG, Aguayo AT, Benito PL, Bilbao J. Role of coke characteristics in the regeneration of a catalyst for the MTG process. *Ind Eng Chem Res*. 1997;36:60–66.
38. Chen D, Moljord K, Fuglerud T, Holmen A. The effect of crystal size of SAPO-34 on the selectivity and deactivation of the MTO reaction. *Microp Mesop Mater*. 1999;29:191–203.
39. Gobin, OC, Retmeier SJ, Jentys A, Lercher JA. Comparison of the transport of aromatic compounds in small and large MFI particles. *J Phys Chem C*. 2009;119:20435–20444.
40. Zhu X, Lobban LL, Mallinson RG, Resasco DE. Tailoring the mesopore structure of HZSM-5 to control product distribution in the conversion of propanal. *J Catal*. 2010;271:88–98.
41. Aguayo AT, Gayubo AG, Ereña J, Olazar M, Arandes JM, Bilbao J. Isotherms of chemical adsorption of bases on solid catalysts for acidity measurement. *J Chem Tech Biotechnol*. 1994;60:141–146.
42. Benito PL, Gayubo AG, Aguayo AT, Olazar M, Bilbao J. Effect of Si/Al ratio and of acidity of H-ZSM5 zeolites on the primary products of methanol to gasoline conversion. *J Chem Tech Biotechnol*. 1996;66:183–191.
43. Benito PL, Gayubo AG, Aguayo AT, Castilla M, Bilbao J. Concentration-dependent kinetic model for catalyst deactivation in the MTG process. *Ind Eng Chem Res*. 1996;35:81–89.
44. Gayubo AG, Arandes JM, Aguayo AT, Olazar M, Bilbao J. Calculation of the kinetics of deactivation by coke in integral reactor for a triangular scheme reaction. *Chem Eng Sci*. 1993;48:1077–1087.
45. Guisnet M. "Coke" molecules trapped in the micropores of zeolites as active species in hydrocarbon transformations. *J Mol Catal A Chem*. 2002;182:367–382.
46. Aguayo AT, Gayubo AG, Vivanco R, Alonso A, Bilbao J. Initiation step and reactive intermediates in the transformation of methanol into olefins over SAPO-18 catalyst. *Ind Eng Chem Res*. 2005;44:7279–7286.
47. Guisnet M, Magnoux P. Organic chemistry of coke formation. *Appl Catal A Gen*. 2001;212:83–96.
48. Aguayo AT, Benito PL, Gayubo AG, Olazar M, Bilbao J. Acidity deterioration and coke deposition in a H-ZSM-5 zeolite in the MTG process. *Stud Surf Sci Catal*. 1994;88:567–572.
49. Benito PL, Gayubo AG, Aguayo AT, Olazar M, Bilbao J. Deposition and characteristics of coke over a HZSM5 zeolite based catalyst in the MTG process. *Ind Eng Chem Res*. 1996;35:3991–3998.
50. Levenspiel K. Suitability of an NTH-Order rate form to represent deactivating catalyst pellets. *Ind Eng Chem Fund*. 1973;12:185–190.

Manuscript received June 23, 2010, and revision received Oct. 1, 2010.